NUCL SCI TECH (2020) 31:45
https://doi.org/10.1007/s41365-020-00752-3

Examining RF jitter and transverse mode-coupling instability in triple-frequency RF systems

Shi-Chang Jiang[1,2] · Gang Xu[1,2]

Received: 3 December 2019 / Revised: 7 March 2020 / Accepted: 11 March 2020 / Published online: 23 April 2020

Abstract A longitudinal accumulation scheme based on a triple-frequency RF system, in which the static radio frequency (RF) bucket is lengthened to be compatible with the realizable raise time of a fast pulse kicker, is proposed in this paper. With this technique, the bunch from a booster can be captured by the longitudinal acceptance without any disturbance to the stored bunch, which remains at the center. This composite RF system consists of three different frequencies, which can be regarded as the conventional bunch lengthening RF system (usually containing fundamental and third harmonic cavities) extended by an additional second harmonic RF cavity. In this paper, we discuss the RF jitter and the transverse mode-coupling instability (TMCI) when using this special RF system. Considering several different bunch profiles, we discuss the beam stability with regard to the RF jitter. However, for the TMCI we assume an ideal bunch profile, where the bunch is exactly lengthened to the maximum extent. While macroparticle simulation is the main method used to study the impact of the RF jitter, numerical analysis and simulations for the TMCI while using a triple-frequency RF system are also presented in this paper. An approximation formula, based on the existing model, is also derived to estimate the impact of the TMCI on the single bunch current threshold when using harmonic cavities.

✉ Shi-Chang Jiang
jiangsc@ihep.ac.cn

[1] Institute of High Energy Physics, Chinese Academy of Sciences, Beijing 100049, China

[2] University of Chinese Academy of Sciences, Beijing 100049, China

Keywords Light source · Triple-frequency · RF jitter · Transverse mode-coupling instability (TMCI)

1 Introduction

One of the intrinsic characteristics of advanced light sources is their narrow dynamic aperture, which creates new challenges for the corresponding injection scheme design [1]. We have previously proposed a new on-axis accumulation scheme based on a triple-frequency radio frequency (RF) system [2], which consists of fundamental, second harmonic, and third harmonic cavities (HCs). Compared to the conventional bunch lengthening RF system, normally consisting of a double-frequency RF system, the added harmonic cavity helps to lengthen the original static longitudinal acceptance. In addition to the time interval between the stored bunch and the outermost injection point, we expect that this value could be larger if the "golf club" effect is taken into consideration [3] by employing the general lattice parameters of fourth-generation light sources. Provided the design of a fast pulse kicker is compatible with this time limitation, in theory there will not be any disturbance to the stored bunch during the injection process. In general, the proposed scheme not only enables on-axis beam accumulation in multi-turns, it also prevents disturbances to the stored bunch and keeps all RF parameters unchanged during normal operation. To study the relevant impacts on the beam while using such a complex RF system, several subtopics are being studied and we will discuss some of them in this paper.

RF jitter is inevitable in the normal operation of an RF system. Even in a high-precision low-level RF (LLRF) system, full elimination is impossible. For SR experiment users requiring high time resolution, investigating and evaluating this effect is very meaningful. Such a complicated triple-frequency RF system may affect the beam stability further.

Macroparticle simulation is our main method of study, where the injection process and normal states are considered separately.

According to their specific bunch profiles, we divide them into a few cases to examine their different features.

Among the collective instabilities restricting the performance of advanced light sources, the single bunch charge is usually constrained by the single bunch instability owing to the interaction between the beam and the transverse impedance. Compared to the instability caused by the other impedance sources, the transverse mode coupling instability (TMCI) is the most harmful to the bunch. Microwave instability (MWI) is a typical longitudinal single bunch instability caused by the interactions between the beam and longitudinal impedance. While in general it can induce bunch turbulence and an increase in energy spread, it may not affect the beam stability immediately, as discussed in [4]. Owing to the small physical aperture of the vacuum chambers in the straight sections (usually only a few millimeters), these large transverse wall (RW) impedances could represent the main contribution of the transverse impedance, and we assume that this instability is predominant in this study. Because of its significance, this instability in a single-frequency RF system has been well solved, simulated, and observed in running systems [5, 6].

An increasing number of modern light sources choose to include harmonic cavities to mitigate the IBS effect and increase the beam’s lifetime. Nonlinear synchrotron motion creates a few new difficulties, and the problem is not well understood. In 1983, Chin studied this problem using perturbation theory and conventional mode-analysis methods [7], proposing that transverse motion will be unstable under any current without radiation damping. S. Krinsky proposed several approximation formulas for different impedance sources, indicating a reduction of the single bunch threshold occurs when harmonic cavities are used [8]. This result is similar to M. Venturini’s conclusions using the typical parameters of a fourth-generation light source, indicating that the presence of harmonic cavities will reduce the instability current threshold by more than a factor of two [9]. However, the simulation results reported in [4] did not indicate a significant impact on the single bunch current threshold when using harmonic cavities, in allusion to the use of a high-energy photon source (HEPS). Additionally, these studies do not involve a triple-frequency RF system, and we therefore investigate this instability under these conditions in this study.

In this paper we discuss the numerical analysis and simulation results in a triple-frequency RF system, which is mainly based on the same framework as a double-frequency RF system using a modified q parameter. The common method is still based on the mode analysis of the linearized Vlasov equation, and we follow M. Venturini’s treatment of the radial dependence of the modes by representing them as values on the simulation grids. From a qualitative analysis through comparison with a conventional double-frequency RF system, single-particle motion can be described through a Hamiltonian similar to that of a quartic potential if we eliminate the first two derivatives of the RF voltage at the synchrotron phase.

Furthermore, based on the existing model, an approximation formula can be derived after several simplifications, and we utilize this formula to estimate the TMCI impact on the single bunch current threshold when harmonic cavities are present. Relevant comparative results with the results from the macroparticle simulation code exhibit good agreement.

The main contents of this paper are divided into five sections. In Sect. 2, we introduce the background of the triple-frequency RF system used for the on-axis beam accumulation to describe the starting point used to build such a complex RF system. In Sect. 3 we differentiate several cases according to the bunch profiles and then present the relevant results using a macroparticle simulation code, and finally provide generalized summaries. We then focus on the TMCI driven by the RW of the RF system in Sect. 4. We first introduce single-particle motion including the triple-frequency RF system and present several pivotal formulas. We then apply M. Venturini’s model to our problem and present the final numerical results. In Sect. 5, we derive the approximation formula from the results obtained in Sect. 4, predicting the impact on the instability threshold with and without harmonic cavities, and relevant benchmarks will be presented. Finally, we conclude the paper.

2 Brief introduction to the triple-frequency RF system

We present a brief introduction to our newly proposed on-axis injection scheme, which is based on a triple-frequency RF system [2]. Sufficient time to raise the full-strength of a kicker pulse, and no disturbance to the circular bunch, are essential to enable beam accumulation. However, these goals are unrealistic in present RF systems, whether using single-frequency or double-frequency systems owing to the fact that the length of one static bucket is insufficient to raise a full kicker pulse.

The improved scheme, by adding another harmonic cavity in the conventional double-frequency RF system (turning it into a triple-frequency system), will significantly lengthen the original longitudinal static bucket. In Fig. 1 we present a comparison while using different HEPS lattice parameters [10], where different colored lines represent the single-frequency, double-frequency, and triple-frequency RF system.

The static bucket formed by the triple-frequency RF system (red lines) is clearly much longer in the longitudinal scale than the other two RF systems. The time limit for the fast pulse kicker is looser [11], and the bunch from an injector through the beam transport line can be kicked and captured by the longitudinal acceptance with no disturbance to the original stored beam if a full pulse can be raised properly.

Flexible bunch lengthening conditions can be satisfied through various RF settings to mitigate the IBS effect and other collective instabilities. Noting that the above figure and following simulation studies are all based on HEPS, we present all major parameters in Table 1, where 14 insertion devices designed for radiation damping in the first stage are included.

3 Impacts of RF jitter on the triple-frequency RF system

Longitudinal motion of an ultra-relativistic electron obeys the following differential equations:

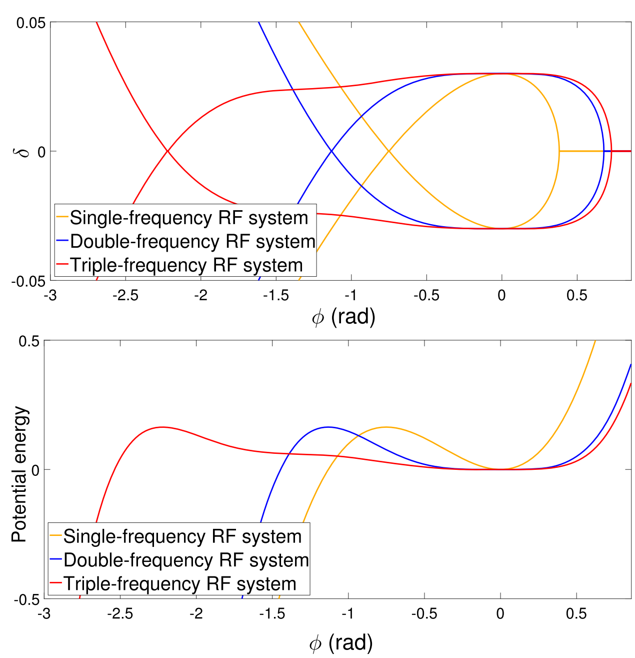

Fig. 1 (Color online) Various static buckets and potential energy curves using different RF systems. The single-frequency, double-frequency, and triple-frequency RF systems correspond to orange, blue, and red lines, respectively

Table 1 Major parameters of HEPS

Parameters	Values
Circumference, C (m)	1360.4
Beam energy, E_0 (GeV)	6
Beam current, I_0 (mA)	200
Natural emittance, ϵ_0 (pm)	26.14
Betatron tunes, ν_x/ν_y	114.19/106.18
Momentum compaction, α_c	1.28e−5
Natural energy spread, σ_d	1.14e−3
Energy loss per turn, U_0 (MeV)	4.38
Damping time, $\tau_x/\tau_y/\tau_z$ (ms)	7.4/12.4/9.5
Harmonic number, h_0	756
Main RF frequency, f_{RF} (MHz)	166.6
Main RF cavity voltage, V_{f} (MV)	7.16
Second harm. cavity voltage, V_{n_1} (MV)	3.59
Third harm. cavity voltage, V_{n_2} (MV)	0.90
Main RF cavity phase, ϕ_{f} (rad)	2.43
Second harm. cavity phase, ϕ_{n_1} (rad)	0.11
Third harm. cavity phase, ϕ_{n_2} (rad)	4.03
Bunch length (no HCs), σ_{z0} (mm)	2.6
Bunch length with HCs, σ_z (mm)	32.2
Linear synchr. tune (no HCs), ν_{s0}	1.2e−3
Avg. synchr. tune with HCs, $\langle\nu_s\rangle$	7.85e−5
ID length, L_{RW} (m)	84
Vacuum chamber radius, r (mm)	3

Energy loss per turn and relevant parameters induced by 14 insertion devices are listed, whose values are derived from ELEGANT simulations [12]

$$\frac{\mathrm{d}z}{\mathrm{d}t} = -c\alpha\delta, \qquad \frac{\mathrm{d}\delta}{\mathrm{d}t} = \frac{1}{E_0 T_0}(eV(z) - U_0). \tag{1}$$

In the equations, c is the speed of light, α is the momentum compaction factor, and δ is the relative momentum deviation. E_0 is the nominal beam energy, T_0 is the revolution time, $V(z)$ is the total RF voltage, and U_0 is the energy loss per turn. When using the triple-frequency RF system [13],

$$V(z) = V_{\mathrm{f}} \sin(\omega_{\mathrm{f}} \frac{z}{c} + \phi_{\mathrm{f}}) + V_{n_1} \sin(\omega_{\mathrm{f}} \frac{z}{c} n_1 + \phi_{n_1}) + V_{n_2} \sin(\omega_{\mathrm{f}} \frac{z}{c} n_2 + \phi_{n_2}), \tag{2}$$

in which ω_{f} is the angular frequency, and n_1, n_2 are the harmonic numbers. V_{f}, V_{n_1}, and V_{n_2} are main and other harmonic cavity voltages.

We first determine whether jitter can affect the original normal injection process, specifically when the bunch is merging toward the center of the static bucket. Then for the normal state, according to the different bunch profiles, we divide them into three cases based on tuning the RF cavity phases:

1. RMS bunch length is less than the maximum, while the bunch profiles are still in a Gaussian distribution;
2. Bunch profiles are non-Gaussian but double-peaked, and there are no distinct bunches;
3. Bunch profiles are double-peaked, but two distinct bunches are formed.

Furthermore, we subdivide each case to obtain a larger sample size by tuning the fundamental cavity phase and third harmonic cavity phase. Figure 2 shows the beam longitudinal distributions corresponding to the three cases from top to bottom, respectively.

The macroparticle simulation code ELEGANT [12] is utilized, and we choose the HEPS lattice for the triple-frequency RF system. The RF jitter white noise from preliminary RF design is shown in Fig. 3, in which random noise will be added to the original RF parameters on a turn-by-turn basis. Here the expected value is 0.01 for amplitude and 0.02° for phase fluctuation [14].

Figure 4 shows the jitter of the bunch centroid after the bunch is injected 2 ns away from the synchrotron phase, while in the right figure, noise is injected from outside the static bucket with a larger time interval of 2.2 ns. The red line and the blue line indicate the trajectories as the bunch is merging toward the center of the static bucket, with and without RF jitter, respectively. The figure indicates no obvious impact to the original trajectory under the present noise data, as the damping motion is not affected. The longitudinal damping time is 9.5 ms, corresponding to approximately 2100 turns. After nearly 10,000 turns, the bunch has concentrated at the center.

Figures 5, 6, 7, and 8 present the relevant results for cases 1, 2, and 3, respectively. In these figures, the maximal offset of the bunch centroid and the bunch length as

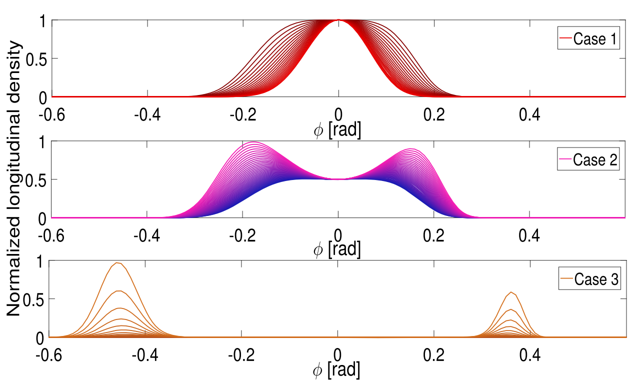

Fig. 2 (Color online) Bunch profiles for cases 1, 2, and 3 from top to bottom, respectively. The lines in each figure represent the same case but involve slightly different tuning RF phases in the fundamental cavities

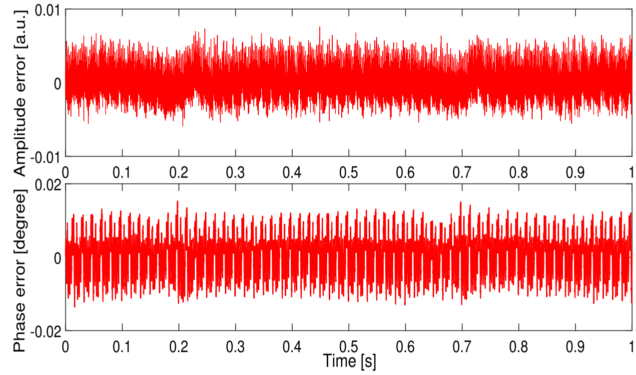

Fig. 3 (Color online) RF jitter white noise data utilized as input in the simulations

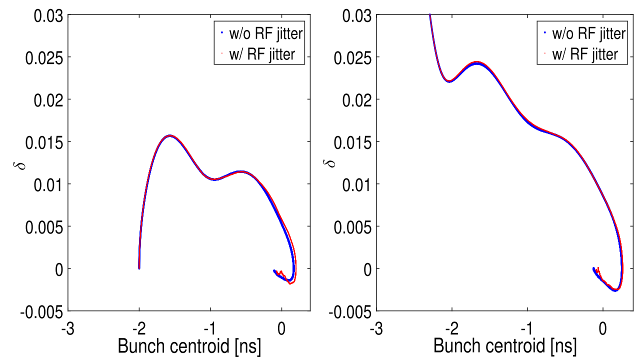

Fig. 4 (Color online) Longitudinal motion of bunch centroid in the presence of RF jitter, injecting at d$t = -2$ ns and d$p = 0$ (left), and at d$t = -2.2$ ns and d$p = 0.03$ (right). Red and blue lines represent the result with and without RF jitter, respectively

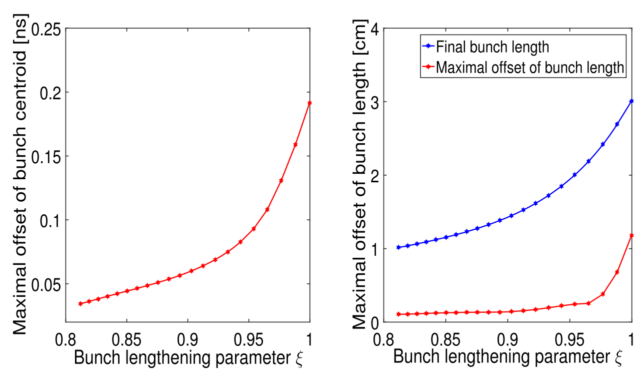

Fig. 5 (Color online) Maximal offset of bunch centroid and bunch length in case 1, discrete points indicate different values of bunch lengthening parameter ξ

they vary with the bunch lengthening parameter ξ are presented, where ξ is defined as

$$\xi = (V_{\mathrm{f}} \cos(\phi_{\mathrm{s}} + \phi_{\mathrm{f}}) + n_1 V_{n_1} \cos(n_1 \phi_s + \phi_{n_1}))/(-n_2 V_{n_2} \cos(n_2 \phi_{\mathrm{s}} + \phi_{n_2})), \tag{3}$$

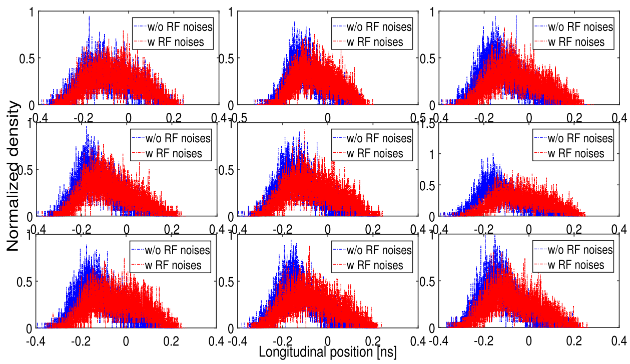

Fig. 6 (Color online) Longitudinal distribution with and without RF jitter for every 2000 turns in each subplot (case 1)

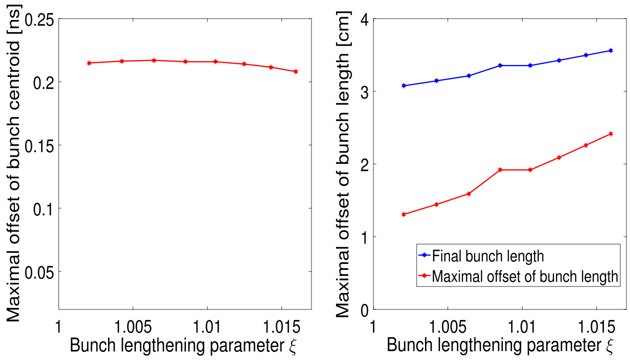

Fig. 7 (Color online) Maximal offset of bunch centroid and bunch length in case 2, discrete points represent different values of bunch lengthening parameter ξ

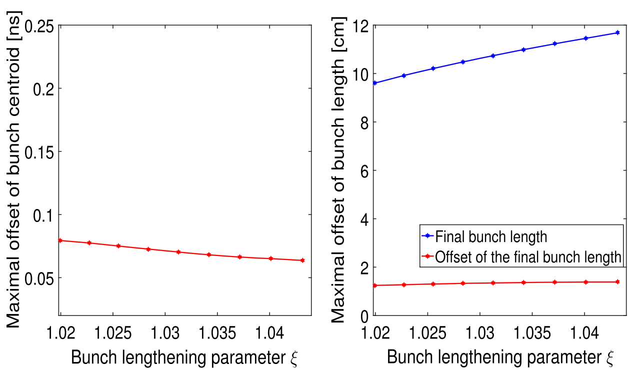

Fig. 8 (Color online) Maximal offset of bunch centroid and bunch length in case 3, discrete points indicate different values of bunch lengthening parameter ξ

and $\xi = 1$ when the first derivative of the RF voltage is zero. Our starting point is the optimal bunch lengthening (OBL) condition, where the first and second derivatives of the RF voltage are both zero. The deviation caused by ξ is away from the OBL condition, and this value is lower for a shorter bunch length.

From Fig. 5, we find that the amplitude of the bunch centroid jitter and the bunch length is decreasing along with a lower ξ, which can also be derived from the longitudinal bunch distribution. When ξ is less than 1, namely the OBL condition, the bunch will be confined within a more narrow potential well and requires more energy to escape this well. Therefore, the bunch is somewhat more stable at this point.

The bunch longitudinal distributions with and without RF jitter are presented in Fig. 6 for every 2000 turns in case 1, in which the bunch is moving forward and backward, indicating that the bunch centroid is shifting. From this perspective, a few deviations to the OBL condition are beneficial against the RF jitter. Nevertheless a shorter bunch length means that stronger beam intensity is needed, which may indicate that a better trade-off between the beam stability and bunch lengthening should be explored.

Figure 7 presents the results for case 2, where the bunch is over-stretched, corresponding to the double-peaked bunch profile. The amplitude of the bunch centroid shift is always greater than 0.2 ns and is larger than in case 1, as is the variation of bunch length, and the change with increasing bunch lengthening parameter ξ is lower. In this case, the bunch is moving in the longitudinal phase space and becomes uncontrollable, which may influence the user experiment, requiring a higher time resolution scale.

For case 3, the result is presented in Fig. 8, which looks like an opposite case compared to case 2. The maximal offsets of the bunch centroid and bunch length are confined within a small range, and no obvious variation tendencies are observed. The bunch is more stable owing to its special double-peaked distribution, where both distinct bunches are confined within two deeper potential wells, which is similar to case 1, although there is no need to lengthen the bunch to such an extreme condition during normal operation of the system.

These simulation results for the RF jitter in a triple-frequency RF system for several different bunch lengthening conditions can be used as references for user experiments that require high longitudinal beam stability. A shorter bunch length will be of benefit to beam stability, while the bunch is in the Gaussian distribution.

In fact, the fundamental cavities are the main power contributors, whether in a double-frequency or a triple-frequency RF system. In our RF setting, the other harmonic cavities are absorbing very little power from the beam. Energy loss per turn U_0 is larger than 4.3 MeV in HEPS, and the bucket height of 3.5% requires more than 7 MV in the fundamental cavities, which may require 5–6 superconducting cavities. For the other harmonic cavities, the designed voltages are only half or less, and less power is exchanged with the beam. Obviously, the fundamental cavities are more easily affected and sensitive to RF jitter. Figure 9 presents the results when removing the RF jitter from the fundamental cavities. The right image only

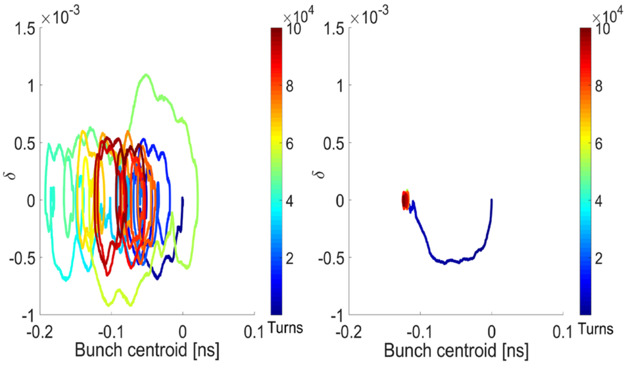

Fig. 9 (Color online) Comparison of the motion of the bunch centroid when removing RF jitter in the fundamental cavities, where the right image shows the result after removing the jitter

includes the noise present in the second and third harmonic cavities. The bunch merges to the synchrotron phase after nearly 10,000 turns, and there are only very weak oscillations in the next 90,000 turns (less than 0.02 ns, as indicated by the warm color area). However, once the fundamental cavities' noise is added, as shown in the left image, the bunch centroid begins to oscillate irregularly over a larger longitudinal scale, where the maximal offset is nearly 0.2 ns. The longitudinal position of the bunch centroid is located at -0.2 ns and 0.02 ns after 30,000 turns and 50,000 turns, respectively.

The problem may be more complicated if the phase transient effect due to the nonuniform filling pattern is taken into consideration, and we may investigate it in the future. The above discussion also applies to a typical double-frequency RF system, in which the fundamental cavities still provide most of the power, while the harmonic cavities absorb little power from the beam. For the conventional single-frequency RF system, there is no need to differentiate the bunch profile to such a complex degree.

4 Relevant studies on TMCI driven by the resistive wall impedance for a triple-frequency RF system

In the following discussion, we examine the transverse mode-coupling instability when using a triple-frequency RF system, namely involving nonlinear synchrotron motion that is slightly different from that of a double-frequency RF system. Note that the Landau damping effect is not considered in the analysis.

Based on the above consideration, the numerical analysis method we use still follows M. Venturini's basic framework [9]. However, certain revisions are required for the triple-frequency RF system regarding the single-particle Hamiltonian and synchrotron motion. In the following discussions, we omit some steps and simply present the revisions to the single-particle motion in a triple-frequency RF system and present several key formulas.

For the OBL condition, the first two derivatives of $V(z)$ will be approximately equal to 0 at the synchrotron phase. If combined with a second radiation power compensation requirement: $V(z) = U_0|_{\phi s}$, these conditions are adequate to solve for all of the RF parameters in the double-frequency case. In this analysis, V_1 is constrained by the required bucket height, while the other three RF parameters $\phi_{\mathrm{f}}, V_n,$ and ϕ_n can be defined as

$$\begin{aligned} \sin\phi_{\mathrm{f}} &= \frac{n^2}{n^2-1}\frac{U_0}{eV_{\mathrm{f}}}, \\ V_n &= \frac{V_{\mathrm{f}}}{n}\sqrt{\cos^2\phi_{\mathrm{f}} + \frac{\sin^2\phi_{\mathrm{f}}}{n^2}}, \\ \cos\phi_n &= -\frac{V_{\mathrm{f}}}{nV_n}\cos\phi_{\mathrm{f}}. \end{aligned} \tag{4}$$

However, it is difficult to represent the triple-frequency RF case this simply because of the degrees of freedom introduced by the additional harmonic number. In Appendix A of [2], we proposed a feasible approach to search for these RF parameters by adding another index and restricted conditions to match the additional degrees of freedom. The final analytic expressions are omitted in this discussion for brevity.

Through the Taylor expansion of Eq. 2, and combining the OBL condition, where the first two derivatives in the Taylor expansion disappear, the third-order term is dominant. To simplify the final expressions, we define a series of auxiliary quantities χ_i, $i = 0, 1, 2, 3, \cdots, n$, where n is the above harmonic number, as $\chi_i = V_{n_i}\cos\phi_{n_i}/(V_{\mathrm{f}}\cos\phi_{\mathrm{f}})$, and $\chi_0 = V_{\mathrm{f}}\cos\phi_{\mathrm{f}}/(V_{\mathrm{f}}\cos\phi_{\mathrm{f}}) = 1$.

The value of n is based on the RF frequency system, in which $\{0, 1\}$ is a conventional bunch lengthening system, and $\{0, 1, 2\}$ is the triple-frequency RF system. Especially for the dualistic combination $\{0, n\}$, χ_n has the concise form $\chi_n = -1/n$ for a positive integer n. For the other multivariate cases, χ_n cannot be expressed so concisely. By means of the auxiliary quantities, we can define a unified V_z up to the third-order term as $V_z = (-1 - n_1^3\chi_1^3 - n_2^3\chi_2^3 - n_3^3\chi_3^3 - \cdots)V_{\mathrm{f}}\cos\phi_{\mathrm{f}}/6$. For a triple-frequency RF system, the first three terms are used. Thus the Hamiltonian of single-particle motion with the quartic potential is $\mathcal{H} = \alpha c\delta^2/2 + \alpha c q z^4/4$, in which

$$q = \frac{(-1 - n_1^3\chi_1 - n_2^3\chi_2^3)}{6}\frac{eV_{\mathrm{f}}k_1^3}{\alpha c E_0 T_0}\cos\phi_{\mathrm{f}}, \tag{5}$$

where k_1 is the wave number. Note that the only difference with the case of the double-frequency RF system is the coefficient q, and we could derive the same results by means of the Hamiltonian; however, we simply present the final formulas. The bunch length with the presence of harmonic cavities and the average synchrotron angular frequency along the bunch can be derived as [9]

$$\sigma_z^2 = \sigma_\delta \frac{2\Gamma(3/4)}{\sqrt{q}\Gamma(1/4)}, \tag{6}$$

$$\langle\omega_S\rangle = \frac{2^{7/4}\pi\alpha c\sigma_\delta}{\Gamma(1/4)^2\sigma_z}. \tag{7}$$

In the equations, σ_δ is the relative energy spread, and $\Gamma(3/4)$ and $\Gamma(1/4)$ are both constants defined by the Gamma function. σ_z and $\langle\omega_S\rangle$ are the bunch length and synchrotron angular frequency when harmonic cavities are present, respectively.

After including the nonlinear synchrotron motion, we follow M. Venturini's basic framework to represent the radial functions $R_m(\rho_n)$ on a uniform grid $\rho_n = (n - 1/2)\Delta\rho_n$, and the similar discretized equation applied is $(\Delta\hat{\Omega})\mathbf{R} = M\mathbf{R}$, in which $\Delta\Omega = (\Omega - \omega_y)/(h_2\langle\omega_s\rangle)$, $h_2 = 2^{3/4}\pi^{3/2}/\Gamma(1/4)^2$, and $\langle\omega_S\rangle = 2\pi\langle\nu_S\rangle/T_0$ are a complex frequency shift and an average synchrotron angular frequency, respectively. The kernel matrix M can be written as [9]

$$\begin{aligned} M_{m,m',n,n'} &= m\rho_n\delta_{m,m'}\delta_{n,n'} \\ &\quad - i\hat{I}e^{-h_1\rho_n^4}\mathcal{G}_{m,m'}(\rho_n,\rho_{n'})\rho_{n'}^2\Delta\rho, \end{aligned} \tag{8}$$

involving the dimensionless bunch current parameter $\hat{I}$, and the constant $h_1 = 2\pi^2/\Gamma(1/4)^4$. Note that all our discussions to this point are in allusion to a single impedance source strictly: the resistive wall (RW), and under this case, the matrix element $\mathcal{G}_{m,m'}$ containing the impedance part can be expanded to a general expression [9].

$$\begin{aligned} \mathcal{G}_{m,m'}(\rho_n,\rho_{n'}) = i^{(m-m')}\int_{-\infty}^{\infty} J_m(\kappa\rho_n)J_{m'}(\kappa\rho_{n'}) \\ \frac{\mathrm{sign}(\kappa) - i}{\sqrt{|\kappa|}}\mathrm{d}\kappa \end{aligned} \tag{9}$$

The RW impedance $Z(k)$ for a round chamber along a total length L is [5]

$$Z(k) = \int_L \beta_y(s)\frac{\mathrm{sign}(k) - i}{\pi b(s)^3}\sqrt{\frac{Z_0\rho(s)}{2|k|}}\mathrm{d}s, \tag{10}$$

where Z_0 is the impedance of free space $Z_0 = 1/(\epsilon_0 c)$ with the vacuum permittivity ϵ_0, and the segmented resistivity is noted as $\rho(s)$. The above dimensionless bunch current parameter is defined as [9]

$$\hat{I} = \frac{Nr_c c\beta_y L}{\pi^{5/2}\gamma\langle\nu_S\rangle b^3\sqrt{c\sigma_c\sigma_z}2\pi}, \tag{11}$$

where N is the number of electrons in a single bunch and r_C is the electron classic radius. The average beta function is β_y, and a circular cross-sectional pipe is defined by its length L, radius b, and conductivity σ_C. Thus far we have listed the required key formulas for the following numerical analysis, although most are those used for a double-frequency RF system except for the difference introduced by q in Eq. 5.

The conventional method is to ascertain all the RF cavity voltages and phases for the OBL condition using the triple-frequency system according to the designed lattice parameters and bucket height. Accordingly χ_1, χ_2, and q are derived, as well as the final bunch length σ_z and the average synchrotron angular frequency $\langle\omega_S\rangle$ from Eqs. 6 and 7. For a specific single bunch current I_b corresponding to the number of electrons N, the RW impedance is considered to derive the final $\hat{I}$ through Eq. 11. After acquiring all indispensable parameters, the final step is to solve the eigenvalues of the kernel matrix M in Eq. 8 and acquire the complex frequency shift $\Delta\hat{\Omega}$ consisting of the disparate transverse modes $\mathrm{Re}\Delta\hat{\Omega}$ and their growth rates $\mathrm{Im}\Delta\hat{\Omega}$.

Numerical analysis results for the TMCI in a triple-frequency RF system are presented in Fig. 10. Unstable motions will emerge at the convergence of the transverse modes $m = 0$ and $m = 1$, and therefore this convergence point identifies the single bunch current threshold I_{th}. The red imaginary line represents the different asymptotic properties $\mathrm{Im}\Delta\hat{\Omega} \propto \hat{I}^6$ for $\hat{I} < 0.2$, and $\mathrm{Im}\Delta\hat{\Omega} \propto \hat{I}$ for higher values, which were previously presented in ***M***. Venturini's results for a double-frequency RF system. Here we consider that this segmented scaling law, and the framework, also applies to the triple-frequency RF system.

We make the comparison utilizing the macroparticle simulation code `ELEGANT` [12]. With this code, the

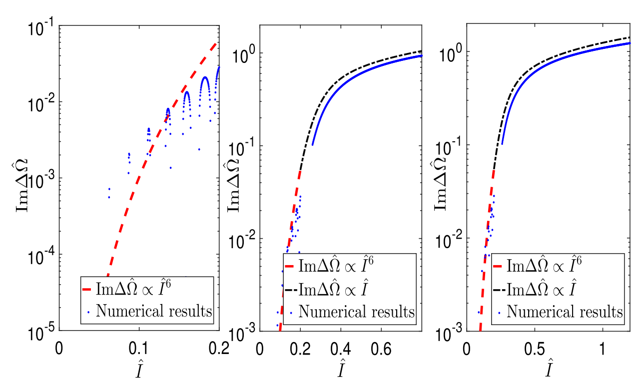

Fig. 10 (Color online) Numerical results and estimated values obtained by applying the scaling law to $\mathrm{Im}\Delta\hat{\Omega}$, represented by blue discrete dots and imaginary lines, respectively. The results obey $\propto \hat{I}^6$ for $\hat{I} < 0.2$ and $\propto \hat{I}$ for values greater than 0.2

ILMATRIX represents a single-turn beam transport, the triple-frequency RF system is built through RFCA, and the RW impedance is given in ZTRANVERSE. By tuning the single bunch charges, the ever-increasing oscillation of the bunch centroid exactly represents the unstable motion. Therefore, the single bunch current threshold and the growth rates by fitting the growth trajectory of the bunch centroid can be derived. Figure 11 presents the comparison between the estimated values obtained by the scaling law and the simulation results. The point of intersection with the radiation damping rate (represented by the blue imaginary line) indicates the single bunch current threshold.

Up to now we have applied the existing theoretical framework of the TMCI in a double-frequency RF system to the triple-frequency system, where the same scaling law is still applicable and the simulation results using ELEGANT fit well. As we discussed previously, both share similar dynamic characteristic and bunch profiles if both remain under the OBL condition. Note that our discussions are all based on the zero-chromaticity condition, and for a different designed chromaticity, this single bunch current limitation may not be as severe.

5 Approximation formula to estimate the impact of TMCI on single bunch current threshold

5.1 Single-frequency RF system

In this section, we present an approximation formula to estimate the impact of the TMCI on the single bunch current threshold. The focus here is the ratio between the single bunch charge threshold including harmonic cavities $Q_{\mathrm{b}}^{\mathrm{harm.}}$, and the original value while using a single frequency RF system Q_{b}^{0}, where their ratio is $Q_{\mathrm{b}}^{\mathrm{harm.}}/Q_{\mathrm{b}}^{0}$.

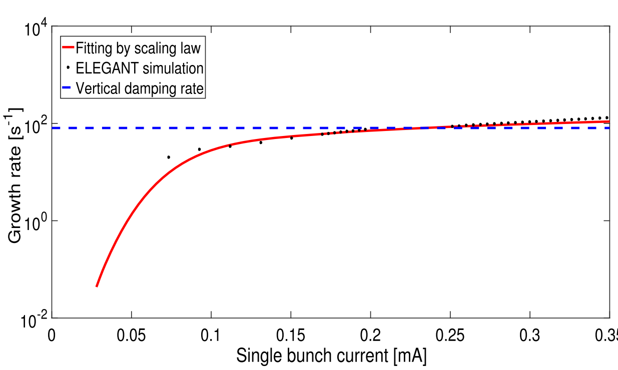

Fig. 11 (Color online) Comparison between ELEGANT simulation and estimated values obtained by fitting the scaling law (black dots and red lines, respectively), while the blue imaginary line indicates the vertical damping rate. The point of intersection at approximately 0.23 mA indicates the single bunch current threshold

When using the expression of the number of electrons N'/N_0, N' is the number of electrons corresponding to the single bunch charge at the threshold as limited by TMCI when harmonic cavities are present, where N_0 corresponds to a single-frequency RF system.

Considering the single-frequency RF system with only linear synchrotron oscillation, the general formula has been deduced in many papers, and we simply choose one of them for our analysis. For the single-frequency RF system, the threshold is determined by [8]

$$\frac{e^2 N_0 \beta_y \kappa}{4\pi\gamma mc^2 \nu_{\mathrm{S}}} = 0.7, \tag{12}$$

where e is the charge of the electron, N_0 has been defined previously, and β_y is the vertical beta function of the impedance. Valid for the case of the above RW wakefield, the kick factor κ_{RW} is approximated as [8]

$$\kappa_{\mathrm{RW}} \approxeq 0.58 \frac{cZ_0 2Ls_0^{3/2}}{4\pi b^4 \sqrt{\sigma_{z0}}}, \tag{13}$$

where $s_0 = 2^{1/3} b^{2/3}/(Z_0\sigma)^{1/3}$, and other parameters have been defined previously. We then substitute the single bunch charge N_0 into the dimensionless bunch current threshold $\hat{I}_0$, eliminating the impact of the RW wakefield, such that $\hat{I}_0 \approxeq 1.707 \frac{\sqrt{2} mr_{\mathrm{C}} c}{e_0^2 Z_0} \equiv 0.1926$. To simplify the discussion, we will utilize this value to determine N_0.

5.2 Including harmonic cavities

We have so far investigated the TMCI for a triple-frequency RF system, indicating it shares similar dynamic characteristics as a double-frequency RF system. The threshold is determined by the growth rate of unstable motion and the vertical damping rate. We next consider that the synchrotron radiation is the only contribution to the damping effect, and this radiation is expressed as

$$\mathrm{Im}\Delta\Omega = \tau_y^{-1}, \tag{14}$$

where $\tau_y = 2E_0 T_0/(J_y U_0)$ is the vertical damping time, and $J_y = 1$ is the radiation damping partition number. Furthermore, based on the fitting function to $\mathrm{Im}\Delta\hat{\Omega}$ presented by M. Venturini in [9],

$$\mathrm{Im}\Delta\hat{\Omega} = \frac{(2^{5/3}\hat{I})^6}{1 + 0.55 \times (4\hat{I})^5 (1 + \tanh(\hat{I}/2))}. \tag{15}$$

Now combining Eqs. 12, 14, and 15, we derive an approximation formula, denoting it as C0. Here we assume that the final $\hat{I}$ is small enough so that we can replace $\tanh(\hat{I}/2)$ with $\hat{I}/2$. We then make a rough approximation to solve the higher-order polynomial equation, where we assume it is located around the dividing point 0.2 and use a multiplying constant to increase the power from $\hat{I}^5$ to $\hat{I}^6$ in the denominator.

For comparison, the formula in [9] is denoted as C1 in the following simulations.

$$\mathrm{C0}: \frac{N'}{N_0} = \frac{a}{(b\langle \nu_s \rangle E_0/U_0 - 1.26)^{1/6}} \sqrt{\frac{\sigma_{z0}}{\sigma_z}}, \tag{16}$$

$$\mathrm{C1}: \frac{N'}{N_0} = 1.15 \times \left(\frac{U_0}{2E_0 \nu_{s0}}\right)^{1/6} \left(\frac{\sigma_{z0}}{\sigma_z}\right)^{1/3}. \tag{17}$$

In these simulations, $a \approx 1.519$ and $b \equiv 4\pi h_2 \approx 8.953$ are both constants, and $h_2 = 2^{3/4}\pi^{3/2}/\Gamma(1/4)^2$. The value on the left side of the equation (greater or less than 1), respectively, indicates a positive or negative impact on the original single bunch current threshold.

The simulation results obtained by ELEGANT using the above equations for C0 and C1 are then implemented and compared. For a more general result, we utilize the lattice parameters from the typical third- and fourth-generation light sources worldwide, whose major parameters are listed in Table 2. The final results are presented in Fig. 12. Note that equation C1 was derived while making a rough approximation based on $\hat{I} < 0.2$; however, for HEPS this value is closer to 0.4, which causes erroneous results in this case. From Fig. 12, the estimated values obtained by C1 therefore diverge from both the simulation results and C0.

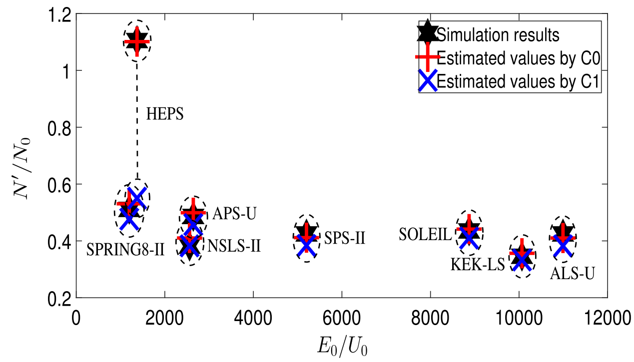

Fig. 12 Comparative results between simulation results and estimated values using approximation formulas C0 and C1

For the other lattice parameters, the estimated values using C0 and C1 fit well with the simulation results. Although there are certain deviations in some points, the overall results agree well with each other. It is somewhat odd that all systems yield a value of N'/N_0 less than 1, which implies a reduction in the single bunch current threshold after including harmonic cavities, except in the

Table 2 Major parameters of some typical third- or fourth-generation light sources, where [a] indicates upgrading projects, while new designs are represented by [b] symbols

Facilities	SPRING8[a]	HEPS[b]	APS-U[a]	NSLS-II	KEK-LS[b]	SOLEIL[a]	SPS-II[a]	ALS-U[a]
Circumference, C (m)	1435.35	1360.4	1103.98	780.3	570.72	354.2	321.3	196.5
Beam energy, E_0 (GeV)	6	6	6	3	3	2.75	3	2
Natural emittance, ϵ_0 (pm)	100	26.14	66.9	510	130	72	960	109
Betatron tunes, ν_x	109.14	114.19	95.125	32.35	48.58	54.30	34.24	41.36
Betatron tunes, ν_y	42.34	106.18	36.122	16.28	17.62	18.30	12.31	20.37
Momentum compaction, α_c	3.32e−5	1.28e−5	5.66e−5	3.68e−4	2.2e−4	1.5e−4	3.18e−4	2.79e−4
Natural energy spread, σ_d	9.26e−4	1.14e−3	9.55e−4	9.8e−4	6.42e−4	8.6e−4	7.7e−4	8.35e−4
Energy loss per turn, U_0 (MeV)	5	4.38	2.27	1.172	0.298	0.31	0.577	0.182
Horizontal damping time, τ_x (ms)	14.4	7.4	12.1	13	29.3	10	9.5	7.7
Vertical damping time, τ_y (ms)	11.5	12.4	19.5	13	38.3	21	11.1	14.4
Longitudinal damping time, τ_z (ms)	5.2	9.5	14.1	6.5	22.7	23.2	6.1	12.8
Harmonic number, h_0	2436	756	1296	1320	952	416	536	328
Main RF cavity voltage, V_f (MV)	7.1	5.28	3.72	4.65	1.75	0.76	1.83	0.63
Third harm. cavity voltage, V_h (MV)	1.57	0.83	0.72	1.49	0.57	0.23	0.58	0.2
Main RF cavity phase, ϕ_f (rad)	2.23	1.94	2.43	2.85	2.95	2.66	2.78	2.81
Third harm. cavity phase, ϕ_h (rad)	− 0.41	− 0.72	− 0.21	− 0.1	− 0.065	− 0.17	− 0.13	− 0.11
Bunch length (no HCs), σ_{z0} (mm)	2.4	3.8	3.7	4.2	3.2	4.6	3.5	3.5
Bunch length with HCs, σ_z (mm)	11.6	25.1	17.1	15.1	13.3	19.1	14.1	14.4
Linear synchr. tune (no HCs), ν_{s0}	3e−3	8.68e−4	2.6e−3	1.08e−2	4e−3	1.6e−3	3.5e−3	2.1e−3
Avg. synchr. tune with HCs, $\langle \nu_s \rangle$	5.05e−4	1.05e−4	4.47e−4	2.4e−3	7.75e−4	3.06e−4	7.16e−3	4.2e−4

Note that relevant data in the table do not necessarily represent the latest versions, and that the bucket height is fixed at 3.5% in a double-frequency RF system consisting of fundamental and third harmonic cavities [15–22]

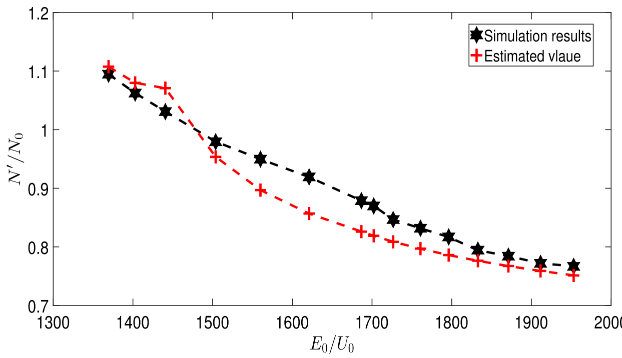

Fig. 13 (Color online) Tuning of E_0/U_0, where the estimated values of N'/N_0 are obtained by approximation formula C0, while the simulation results are obtained from ELEGANT

case of HEPS. This occurs because the E_0/U_0 and ν_S values applied to HEPS are too low, leading to a smaller value after subtracting a constant from the denominator of Eq. 16, which increases the positive contribution to the final N'/N_0. From the perspective of the lattice parameters, the larger energy loss per turn U_0 and very small momentum compaction factor α are both contributing factors.

Here we hypothesize another situation to further study the impact of E_0/U_0. The additional U_0 caused by the insertion devices can be gradually varied while fixing the nominal energy E_0. Other related variables, the radiation damping partition number J_i, the energy spread σ_δ, and the natural emittance ϵ_0 will change correspondingly. For each specific value of E_0/U_0, estimated values are determined by C0 and by simulation results derived from ELEGANT. The results are shown in Fig. 13. Except for a few point deviations, the general trend by the estimation formula C0 fits well with the simulation results. Along with the increase in E_0/U_0, the ratio of the single bunch threshold N'/N_0 decreases from 1 to approximately 0.7.

6 Conclusion

We have presented discussions on RF jitter and TMCI regarding a triple-frequency RF system, and our starting point is to determine whether there is unexpected divergence under this special environment. In terms of a triple-frequency RF system itself, the other two harmonic cavities help to tune the total $V(z)$ and lengthen the original static bucket. Further, the triple system is similar to a conventional bunch-lengthening RF system. As we mentioned in Sect. 3, there is very little power exchange with the beam except for the fundamental cavities. RF jitter is considered important to stabilize the circular bunch, while it is not as crucial for the injection process. As for the continuous shift of the bunch centroid, an effective method to restrain this shift is to control the amplitude of the RF jitter noise.

In terms of the bunch in the environment using a triple-frequency RF system, TMCI is one of the single bunch instabilities, and TMCI's role is similar in a double-frequency RF system. Furthermore, because of the similar longitudinal distribution in both double- and triple-frequency systems, the basic theoretical framework is still applicable, and by applying the approximation formula C0, the impact of the TMCI on the single bunch current threshold of a triple-frequency system can therefore be reasonably estimated.

References

1. D. Einfeld, M. Plesko, J. Schaper, First multi-bend achromat lattice consideration. Synchrotron Radiat. **21**, 856 (2014). https://doi.org/10.1107/S160057751401193X
2. S.C. Jiang, G. Xu, On-axis injection scheme based on a triple-frequency rf system for diffraction-limited storage rings. Phys. Rev. ST Accel. Beams **21**, 110701 (2018). https://doi.org/10.1103/PhysRevAccelBeams.21.110701
3. M. Aiba, M. Böge, F. Marcellini, Á. Saá Hernández, A. Streun, Longitudinal injection scheme using short pulse kicker for small aperture electron storage rings. Phys. Rev. ST Accel. Beams **18**, 020701 (2015). https://doi.org/10.1103/PhysRevSTAB.18.020701
4. H.S. Xu, N. Wang, Influences of Harmonic Cavities on the Single-Bunch Instabilities in Electron Storage Rings. In Proceedings of 60th ICFA Advanced Beam Dynamics Workshop on Future Light Sources, FLS2018, Shanghai, China (IEEE, New York, 2018) pp. 128–132. https://doi.org/10.18429/JACoW-FLS2018-WEP2PT024
5. R.R. Lindberg, Fokker–Planck analysis of transverse collective instabilities in electron storage rings. Phys. Rev. Accel. Beams **19**, 124402 (2016). https://doi.org/10.1103/PhysRevAccelBeams.19.124402
6. G. Skripka, Å. Andersson (Lund U., MAX-lab), F. Cullinan et al., Impedance characterization and collective effects in the MAX IV 3 GeV Ring. In Proceedings of NAPAC2016, Chicago, IL, USA (IEEE, New York, 2016) pp. 843–846. https://doi.org/10.18429/JACoW-NAPAC2016-WEA3CO04
7. Y. Chin, K. Satoh, K. Yokoya, Instability of a bunched beam with synchrotron frequency spread. Part. Accel. **13**, 45–66 (1983)
8. S. Krinsky, Simulation of transverse instabilities in the NSLS-II storage ring. Technical report BNL-75019 (National Synchrotron Light Source, 2005). https://doi.org/10.1097/CAD.0b013e32833d19f0
9. M. Venturini, Harmonic cavities and the transverse mode-coupling instability driven by a resistive wall. Phys. Rev. ST Accel. Beams **21**, 024402 (2018). https://doi.org/10.1103/PhysRevAccelBeams.21.024402
10. G. Xu, X.H. Cui, Z. Duan et al., Progress of lattice design and physics studies on the high energy photon source. In Proceedings of the 9th International Particle Accelerator Conference, IPAC2018, Vancouver, BC, Canada (IEEE, New York, 2018) pp. 1375–1378. https://doi.org/10.18429/JACoW-IPAC2018-TUPMF052
11. H. Shi, J.H. Chen, Z. Duan et al., Fast kicker and pulser R&D for the HEPS on-axis injection system. In Proceedings of the 9th

International Particle Accelerator Conference, IPAC2018, Vancouver, BC, Canada (IEEE, New York, 2018) pp. 2846–2849. https://doi.org/10.18429/JACoW-IPAC2018-WEPML069
12. M. Borland, Elegant: a flexible SDDS-compliant code for accelerator simulation. Technical report LS-287 (Advanced Photon Source, 2000). https://doi.org/10.2172/761286
13. G. Xu, J.H. Chen, Z. Duan et al., On-axis beam accumulation enabled by phase adjustment of a double-frequency RF system for diffraction-limited storage rings. In Proceedings of the 7th International Particle Accelerator Conference, IPAC2016, Busan, Korea (IEEE, New York, 2016) pp. 2032–2035. https://doi.org/10.18429/JACoW-IPAC2016-WEOAA02
14. P. Zhang, X. Hao, T. Huang et al., The 166.6 MHz proof-of-principle SRF cavity for HEPS-TF. In Proceedings of the 8th International Particle Accelerator Conference, IPAC2017, Copenhagen, Denmark (IEEE, New York, 2017) pp. 1049–1051. https://doi.org/10.18429/JACoW-SRF2017-TUPB034
15. H. Ego, T. Asaka, T. Fujita et al., RF system of the SPring-8 upgrade project. In Proceedings of the 7th International Particle Accelerator Conference, IPAC2016, Busan, Korea (IEEE, New York, 2016) pp. 414–416. https://doi.org/10.18429/JACoW-IPAC2016-MOPMW009
16. N. Juntong, T. Chanwattana, K. Kittimanapun et al., Conceptual design of the RF system for the storage ring and linac of the new light source in Thailand. In Proceedings of the 9th International Particle Accelerator Conference, IPAC-2018, Vancouver, BC, Canada (IEEE, New York, 2018) pp. 4505–4508. https://doi.org/10.18429/JACoW-IPAC2018-THPMK087
17. F. Cullinan, R. Nagaoka, G. Skripka et al., Transverse coupled-bunch instability thresholds in the presence of a harmonic-cavity-flattened rf potential. Phys. Rev. ST Accel. Beams **19**, 124401 (2016). https://doi.org/10.1103/PhysRevAccelBeams.19.124401
18. M. Borland, T. Berenc, R. Lindberg et al., Tracking studies of a higher-harmonic bunch-lengthening cavity for the advanced photon source upgrade. In Proceedings of the 6th International Particle Accelerator Conference, IPAC2015, Richmond, VA, USA (IEEE, New York, 2015) pp. 543–545. https://doi.org/10.18429/JACoW-IPAC2015-MOPMA007
19. S. Krinsky, J. Bengtsson, S. Kramer, Consideration of a double bend achromatic lattice for NSLS-II. In Proceedings of EPAC2006, Edinburgh, Scotland (IEEE, New York, 2006) pp. 3487–3489
20. T. Honda, Concept of a new generation synchrotron radiation facility KEK light source. In Proceedings of the 8th International Particle Accelerator Conference, IPAC2017, Copenhagen, Denmark (IEEE, New York, 2017) pp. 2687–2690. https://doi.org/10.18429/JACoW-IPAC2017-WEPAB047
21. A. Loulergue, Baseline lattice for the upgrade of SOLEIL. In Proceedings of 60th ICFA Advanced Beam Dynamics Workshop on Future Light Sources, FLS2018, Shanghai, China (unpublished)
22. D. Robin, Overview of ALS Upgrade, in Low Emittance Rings Workshop 2016, Zurich, Switzerland, October 26–28, 2016 (unpublished)